Surface Characterization of Three Marine Bacterial Strains by Fourier Transform IR, X-ray Photoelectron Spectroscopy, and Time-of-Flight Secondary-Ion Mass Spectrometry, Correlation with Adhesion on Stainless Steel Surfaces

C. M. Pradier,*,† C. Rubio,†,§ C. Poleunis,‡ P. Bertrand,‡ P. Marcus,† and C. Compère§

Laboratoire de Physico-Chimie des Surfaces, CNRS (UMR 7045) ENSCP, 11 rue P&M Curie, F-75005-Paris, France, Université Catholique de Louvain, PCPM, Croix du Sud 1, B-l348, Louvain-la-Neuve, Belgium, and Service Interfaces et Capteurs, IFREMER, BP 70, 29280 Plouzané, France

Received: November 19, 2004; In Final Form: February 28, 2005

Adhesion of bacterial strains on solid substrates is likely related to the properties of the outer shell of the micro-organisms. Aiming at a better understanding and control of the biofilm formation in seawater, the surface chemical composition of three marine bacterial strains was investigated by combining Fourier transform IR spectroscopy, X-ray photoelectron spectroscopy (XPS), and time-of-flight secondary-ion mass spectrometry (ToF−SIMS). The D41 strain surface showed evidence of proteins, as deduced from the NH_2 and NCO XPS and ToF−SIMS fingerprints; this strain was found to adhere to stainless steel, glass, or Teflon surfaces in a much higher quantity (2 orders of magnitude) than the two other ones, DA and D01. The latter are either enriched in COOH or sulfates, and this makes them more hydrophilic and less adherent to all substrates. Correlations with physicochemical properties and adhesion seem to demonstrate the role of the external layer composition, in particular the role of proteins more than that of hydrophobicity, on their adhesion abilities.

Introduction

The colonization of solid surfaces by micro-organisms is a cause of material degradation and considerable economic loss in health, food, or marine environments. The formation and growth of biofilms are strongly dependent on the substrate properties, hydrophilicity,[1] net surface charge, roughness,[2] and oxidation/hydroxylation,[3] but no clear correlation has yet been established between cell adhesion, surface physicochemical properties, and cell surface compositions. Recent works by Van der Mei et al.,[4] Dufrêne et al.[5] from a surface science point of view, and Briandet et al.,[6] Grasland et al.,[7] and Sharma et al.[8] from a microbiological one brought new insights into the chemical composition of the cell surface and demonstrated the role of multiparameters such as hydrophilicity, electron-donor character, or acid−base properties of cells upon their adhesion. Several surface science techniques are often combined to increase the level of knowledge of the external part of the cell. As examples, Rouxhet et al. used atomic force microscopy (AFM) and X-ray photoelectron spectroscopy (XPS) to investigate cell−substratum interfaces;[9] XPS and secondary-ion mass spectrometry (SIMS) were successfully applied by Tyler et al. to get an accurate characterization of polymer surfaces and of biomolecules adhering on them, the difficulty being to address the nature of the functional groups in the adhesion.[10] IR and XPS were shown to be complementary for the characterization of cell-surface composition.[11] A better knowledge of the cell external layer composition is indeed a prerequisite to understand their adhesion behavior on solid surfaces, and this is the objective of the present work based on the use of several and complementary surface analysis techniques; this paper then presents adhesion tests and a discussion on some clear, or less clear, correlation with the characterization of the cell outer shell constituents. Though it is now commonly admitted that different mechanisms of adhesion exist that make it impossible to establish general conclusions about the role of specific parameters,[12] it is worth wondering whether correlations appear between surface compositions of strains having the same original environment and their behavior in contact with solid surfaces.

In the frame of a long-term study of biofilm formation in marine environment, three microorganisms, originating from seawater, were isolated from bacterial populations on stainless steel, glass, and Teflon surfaces after immersion for a few hours in seawater. They are called pioneer bacteria since they are present during the initial stage of a biofilm formation.

Three pioneer bacterial strains, named D01, DA, and D41, were retained for the following reasons: they are nonpathogenic, easy to grow and to handle, and exhibit various characteristics. D41 and DA produce exopolymeric substances, while D01 does not. Viability tests in artificial seawater revealed that DA survives the longest time; the number of viable cells decreases by a factor of 10 after a period of 100 h, whereas it goes down by 3 orders of magnitude for D41 and by 6 orders of magnitude for D01.[13]

An identification by ARN recognition led to the following data:

(1) D01 is a *Vibrio lentus* (98%) and *Vibriolentus sp*-like (96%) micro-organism.

(2) D41 is a *Pseudomonas Alteromonas sp*-like (96%) micro-organism. The final identification of D41 is on its way.

(3) DA is a bacterial stain that has been thoroughly identified; it is an *Alteromonas macleodii subsp. fijiensis* that produces a polymer named "A" that is also well characterized.[14]

D01, DA, and D41 are all Gram-negative bacteria, i.e., partially covered by exopolysaccharides.[15] This suggests the

* To whom correspondence should be addressed. E-mail: claire-marie-pradier@enscp.jussieu.fr. Present address: Laboratoire de Réactivité de Surface, CNRS (UMR 7609), Université P. et M. Curie, 4 Place Jussieu, 75005-Paris, France.

† Laboratoire de Physico-Chimie des Surfaces.

‡ Université Catholique de Louvain.

§ Service Interfaces et Capteurs.

10.1021/jp044705p CCC: $30.25
Published on Web 04/12/2005

probable presence of carboxylic acid groups and phosphates in their outer shells.[16]

Adhesion of the three strains to various solvents was measured in artificial seawater following the microbial adhesion to solvents (MATS) technique recently developed by van Oss et al. and Bellon-Fontaine et al.[17] Four solvents, chloroform, ethyl acetate, decane, and hexadecane, were used, aiming at possibly detecting differences between the three species in terms of electrostatic and hydrophobic interactions. D01 and DA do have a strong electron-donor and electron-acceptor character; in the absence of strong electrostatic interactions, one can say that D01 and D41 are hydrophilic.[18,19] D41 adheres to all solvents, polar or not, acidic or not, showing weak electron-donor and weak electron-acceptor character; this strain is likely to be less hydrophilic than the two others.[13]

Fourier-transform IR (FT-IR), XPS, and time-of-flight (ToF) SIMS, three techniques having different sensitivities and analysis depths, were combined to characterize the chemical composition of the topmost layers of the micro-organisms. XPS and FT-IR, in the reflection mode (FT-IRRAS), were also used to characterize surfaces of stainless steel substrates after adhesion of the three studied bacteria in artificial seawater. Adhesion on solid surfaces was quantified by epifluorescence microscopy, and attempts were made to correlate results of these adhesion tests to the surface characterization of the three strains. Although XPS and ToF−SIMS, operated under vacuum conditions, may alter the conformation and possibly the external composition of the cells, significant correlations were observed.

Experimental Section

Bacterial Cell Preparation. Bacterial cells were grown in Marine Broth (Difco laboratories) to the stationary phase; the solutions were then filtered and centrifuged. Cells were separated from the supernatant by centrifugation and placed in sterile artificial seawater; they were then centrifugated and placed again in artificial seawater. The so-washed material was then placed again in sterile artificial seawater, and the optical density was adjusted to 0.8 at 400 nm ($\sim 10^8$ CFU/mL). The solutions were then frozen at −20 °C and freeze dried following a procedure well established by other authors.[20]

The obtained powders were pressed on an ultrahigh-vacuum-compatible adhesive tape for XPS analyses. They were pressed together with KBr to make pellets for IR transmission analyses. This mode of analysis gave better results than IR in the attenuated total reflection (ATR) mode. For the ToF−SIMS measurements, the powders were pressed with a spatula on conductive silver double-face tape (SPI #5070).

Adhesion Tests. For the adhesion tests, AISI 316 stainless steel substrates, cleaned by a procedure previously described,[21] were immersed, horizontally, in an agitated solution of bacteria (10^8 CFU/mL) in sterile artificial seawater; coupons were rinsed in three successive baths in sterile artificial seawater under controlled, gentle stirring to remove less strongly adhering cells. The total number of bacteria retained on the surface was directly estimated on a first set of substrates using an epifluorescence microscope after staining with a fluorochrome (orange acridine 0.01% m/v). On other surfaces, bacterial cells were detached in sterile artificial seawater by using a sonication bath for 2 min. Then, viable total cells were counted after incubation of this bacterial suspension on marine agar by using the serial dilution spreading technique.

Each experiment was performed in triplicate by using independently prepared cultures.

Eventually, another series of samples were then frozen at −20 °C, submitted to freeze drying overnight, and stored in sterile boxes at room temperature until the surfaces were analyzed by ToF−SIMS, XPS, or FT-IRRAS.

FT-IR Analyses. Pure bacterial powder were analyzed by FT-IR in the ATR mode on a ZnSe crystal. KBr pellets (KBr 220 mg + bacterial powder 1 mg) were also prepared and analyzed in transmission IR to get a better spectrum of the bacteria in the lower wavenumber range. A NICOLET Magna 550 IR spectrometer with a mercury cadmium telluride (MCT) wide-band detector was used for these analyses.

They provided a characterization of the entire cell, not a surface specific analysis, but it was helpful for some attributions of the chemical groups possibly present in each of the macromolecules.

FT-IRRAS for analyses of the stainless steel surfaces after cell adhesion were carried out using the reflection mode at a grazing incidence (6°). A FT-IR spectrometer (Nicolet, Magna 550) with a MCT wide-band detector was used. A typical spectrum was obtained by averaging the signal of 800 scans at a resolution of 4 cm^{-1}. All spectra were ratioed against a background spectrum recorded on a sample which had been cleaned as mentioned above.

Surface Analysis by XPS. The XPS analyses were performed with a VG ESCALAB Mk II spectrometer, using the Al Kα X-ray source (1486.6 eV). A 20-eV pass energy was applied for analyzing the following core level regions: O 1s, C 1s, S 2p, and N 1s. The binding energies were calibrated against the binding energies of Au $4f_{7/2}$ and Cu $2p_{3/2}$; with this calibration and after correction of the charge effect, the low-energy carbon peak, attributed to hydrocarbon contamination, was set at 284.8 ± 0.1 eV. The sensitivity factors of the elements were taken from ref 22, and the transmission factor was checked to be constant over the analyzed range. In the fitting procedure, no constraint was applied to the initial binding energy values, and the full width at half maximum (fwhm) was set at 1.4 ± 0.2 eV for the carbon and nitrogen contributions and 1.6 ± 0.2 eV for the oxygen contributions, with a Gaussian/Lorentzian ratio, G/L, equal to 80/20.

Let us recall that XPS gives an elemental and, possibly, a functional analysis of the cell surfaces, with an analysis depth of 3−5 nm.[23]

Surface Analysis by ToF−SIMS. The ToF−SIMS spectra measurements were performed with a PHI-Evans TFS-4000MMI (TRIFT 1) spectrometer.[24] The sample was bombarded with a pulsed $^{69}Ga^+$ ion beam (15 keV, 940 pA direct current, 11 kHz frequency, and 22-ns unbunched pulse width). To increase the detection efficiency of high-mass ions, a 7-keV post-acceleration was applied at the detector entry. The analyzed area was a square of 120 μm × 120 μm. With a 5-min data acquisition time, the fluence was about 1.8×10^{12} ions/cm^2, which ensured static conditions.[25] For the present samples and analytical conditions, the mass resolution was about 3000 at $m/z = 41$ ($C_3H_5^+$ peak). Charge effects were compensated by means of a pulsed electron flood gun ($E_k = 24$ eV).

The ToF−SIMS relative intensities were determined according to the following calculation procedure:

- for the organic positive secondary ions,

$I_{rel} = 100 \times I_x/\{I_{tot} - (I_H + I_{Na} + I_{Mg} + I_K + I_{Ca})\}$;

- for the inorganic positive secondary ions,

$I_{rel} = 100 \times I_x/I_{tot}$;

- for the organic negative secondary ions,

$I_{rel} = 100 \times I_x/\{I_{tot} - (I_H + I^{35}_{Cl} + I^{37}_{Cl})\}$;

- for the inorganic negative secondary ions,

$I_{rel} = 100 \times I_x/(I_{tot} - I_H)$;

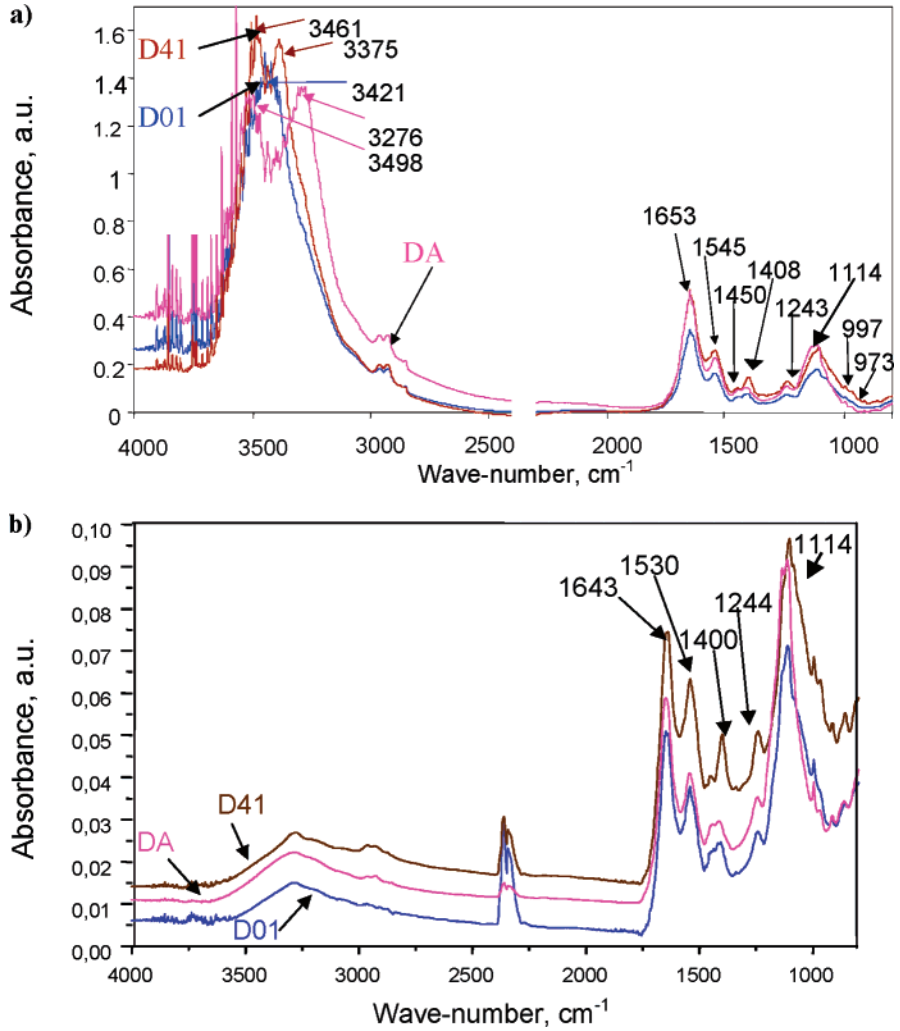

Figure 1. FT-IR spectra of the three bacteria: (a) transmission mode through KBr pellets; (b) ATR mode on a Ge crystal.

where I_x represents either the area of the peak "X" or the sum of the areas of several peaks related to a same chemical function.

SEM Analyses. A Hitachi S-3200N scanning electron microscope was used for analyzing solid surfaces with adhering material.

After immersion in bacterial solutions, the samples were successively rinsed in artificial seawater plus 2.5% glutaraldehyde then artificial seawater plus pure water, decreasing the fraction of salts; they were eventually rinsed in water−ethanol solutions, the concentration of ethanol increasing from 0 to 100% progressively to avoid cell destruction; the surfaces were then covered with a thin (200−300 Å) layer of gold. This technique provided us with the total number of adhering cells (detection limit: 10^4 cells/cm^2).

Results

1. Analysis of the Bacterial Strains. a. FT-IR Results. IR spectra of the three strains are shown in parts a and b of Figure 1. The former was obtained by analysis of the powders in the ATR mode, the signal over noise ratio is better at higher wavenumbers, whereas the latter come from IR analysis through a KBr pellet, more sensitive in the lower wavenumber range.

A large set of bands appear on the three spectra, at positions characteristic of proteins (1640, 1540, and 1240 cm^{-1}, corresponding to amides I, II, and III, respectively), carbohydrates (1114 and 1400 cm^{-1}), and possibly sulfates (ca. 1100 cm^{-1}).[26,27] Let us note slight spectral differences in the 3200−3500-cm^{-1} region: a band at 3276 cm^{-1}, only present on the DA spectrum, while the two other cells absorb at higher wavenumbers, 3275 and 3460 cm^{-1}. It is particularly difficult to interpret these slight differences in the region where NH and OH stretch vibrations are present and possibly shifted by humidity or intramolecular interactions.

b. XPS Results. The survey scans, 20−1100 eV (spectra not shown), reveal that the three cell surface layers (2−5 nm) are mainly constituted of C, O, and N, with low levels of S, P, Na, and Cl. The presence of NaCl is related to the preparation of the bacteria.

Figure 2 shows the C 1s and N 1s regions of the three micro-organism surfaces.

At first view, although a large charge effect shifts the carbon peaks to higher binding energy, the shape and intensity of the C 1s peak are obviously different from one cell to another. Differences are even clearer on the N 1s peaks. Noticeable is the weaker N 1s peak for the DA compared to the two others (see in Table 1). As an example, the peak-fitting results for the C 1s, O 1s, and N 1s peaks of the DA micro-organism are given in Figure 3. For the three cells, the C 1s spectra were decomposed into four contributions centered, after charge correction, at 284.8 ± 0.2 eV for carbon singly bonded to carbon and hydrogen, 286.3 ± 0.4 eV for carbon singly bonded to oxygen or nitrogen, 287.8 ± 0.4 eV for carbon doubly bonded to oxygen or simply bonded to two oxygen atoms, and a fourth contribution at E_B > 289 eV for carbon in COOH groups. The

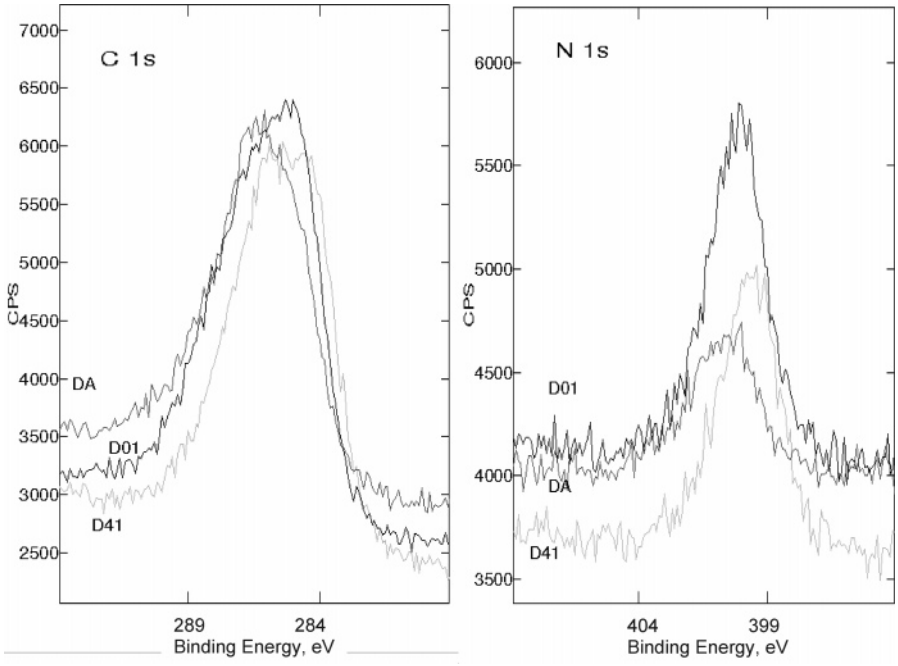

Figure 2. C 1s and N 1s XPS spectra of the three bacteria, measured after freezing and freeze-drying of the cells. The spectra are shown as recorded, with no charge correction on the EB values.

TABLE 1: Elemental Composition (Oxygen, Nitrogen, and Sulfur vs Total Carbon Molar Ratio) and Contributions (Peak Intensities) to the XPS C 1s, O 1s, and N 1s Peaks from the XPS Analyses of the 3 Cells

	O/Ctot	N/Ctot	S/Ctot
D01	0.29	0.16	0.02
DA	0.47	0.11	0.11
D41	0.34	0.16	0.05

	C 1s				O1s			N1s		S 2p
BE, eV	284.8 ± 0.2	286.3 ± 0.4	287. 8 ± 0.4	289. 5 ± 0.3	531.5 ± 0.3	533.1 ± 0.4	534.1 ± 0.4	400.3 ± 0.2	402 ± 0.2	169 ± 0.5
D01	4194	4565	3767	2649	4765	6101	1873	2513	1648	565
DA	5295	5474	1987	371	7050	3850	2770	1198	914	2 103
D41	4782	4635	4292	1367	11 764	7050	449	2540	1463	1 268

fractions of each type of carbon is very much dependent on the nature of the cell (see Table 1).

The contribution at ca. 287.8 eV might originate from aldehydes, acetals, or amides. We exclude the two first possibilities in view of the IR spectrum that shows no absorption either at 1720 or around 2820 cm^{-1}, those wavenumbers being expected for aldehydes and acetals, respectively. The O 1s peak was best fitted with three contributions, after charge correction, at 531.5 ± 0.3, 533. 1 ± 0.4, and 534.1 ± 0.4 eV, respectively. The first one may originate from several groups, C═O or P═O functions, the second one to C−OH, P−OH, and C−O−C, and the last one to water molecules, trapped in the bacterial strains, or to sulfates.

The N 1s peak was fitted with two contributions, after charge correction, at 400.3 ± 0.2 and 402 ± 0.2 eV, respectively. The former one is attributed to nitrogen in amine or amide functions, whereas the latter is more likely due to nitrogen in protonated NH_x^+ groups.

The S 2p peaks were all centered at 169.8 ± 0.4 eV, a binding energy indicating the presence of sulfates on the surface.

The O1s, N 1s, and S 2p intensities vs the one of carbon, as well as the intensity of each contribution to the C 1s, O 1s, and N 1s peaks of the three cells, make clear the following main points:

(1) The oxygen and sulfur peaks were the highest on the DA strain;

(2) The amounts of nitrogen were very similar on D01 and D41, higher by a factor of two than on DA.

The peak fitting of the C 1s peaks also revealed interesting differences: the high BE contribution, at 289.5 eV, was by far the most intense for D01, whereas the highest C═O, N−C═O, or O−C−O contributions (287.8 eV) were observed on D41. A slightly higher fraction of aliphatic carbon was observed on DA compared to the two other cells.

Similarly, for the contributions to the O1s peak, the one originating from C═O or P═O functions is strongly dominating on the D41 strain, whereas those attributed to C−OH or P−OH do have similar intensities on D01 and D41, slightly higher than on DA.

c. ToF−SIMS Results. The positive-ion ToF−SIMS spectra shown in Figure 4 correspond to the D01, D41, and DA strains, respectively (mass range from 0 to 100 *m*/*z*). The Y scales were saturated due to the huge intensities of the Na^+, Mg^+, and K^+ cations coming from the sea salts. Their absolute intensities are reported below the figures. For these cations, there are no major differences between the three bacterial strains, the lowest alkali ion intensities being observed for DA.

In the three bacterial strain spectra, a series of peaks coming from the combination between Na and other inorganic elements such as O, S, K, and Cl are observed at the masses 45.98, 62.81, 83, and 99 *m*/*z*; they correspond to Na_2^+, Na_2O^+, Na_2Cl^+, and

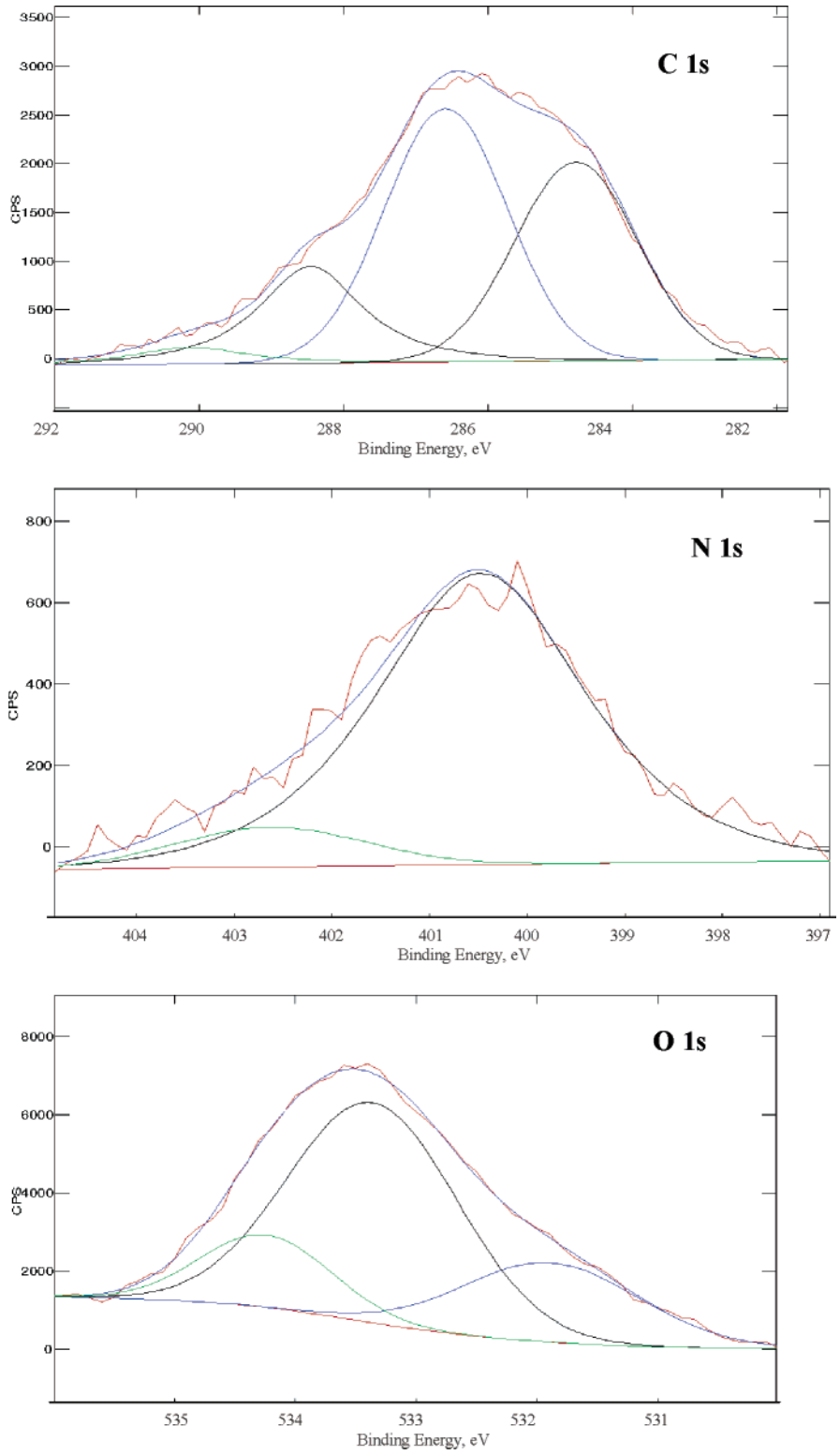

Figure 3. Decomposition of the C 1s, N 1s, and O 1s peaks of the DA strain.

$NaKCl^+$, respectively. Some other peaks are detected at higher masses (not shown); these are: $Na_3Cl_2^+$, $Na_3SO_4^+$, and $Na_3SO_5^+$.

Many aliphatic and aromatic hydrocarbon peaks ($C_xH_y^+$) are detected. The aliphatic peaks are observed at 15, 27, 29, 41, 43, 55, 57, 69, 71, ... *m*/*z* and the aromatic at 50, 51, 77, 91, ... *m*/*z*. The hydrocarbon peak intensities are similar on the D01 and D41 bacterial strains and higher on DA.

Other organic compounds are also detected. On one hand, the oxygenated peaks at masses 31.02, 45, 59, and 73 *m*/*z* are ascribed to CH_3O^+, $C_2H_5O^+$, $C_3H_7O^+$, and $C_4H_9O^+$, respectively. On the other hand, the nitrogenized peaks at masses 17, 18, 30, 31.04, 44, 46.07, 58, 72, 84, and 86 *m*/*z* correspond to NH_3^+, NH_4^+, CH_4N^+, CH_5N^+, $C_2H_6N^+$, $C_2H_8N^+$, $C_3H_8N^+$, $C_4H_{10}N^+$, $C_5H_{10}N^+$, and $C_5H_{12}N^+$, respectively. It is important to note that all these nitrogenized peaks are weak, the weakest ones being on the DA bacterial strain.

The negative-ion ToF−SIMS spectra shown in Figure 5 correspond to the D01, D41, and DA strains, respectively (mass range from 20 to 100 *m*/*z*). Because of the huge intensities of

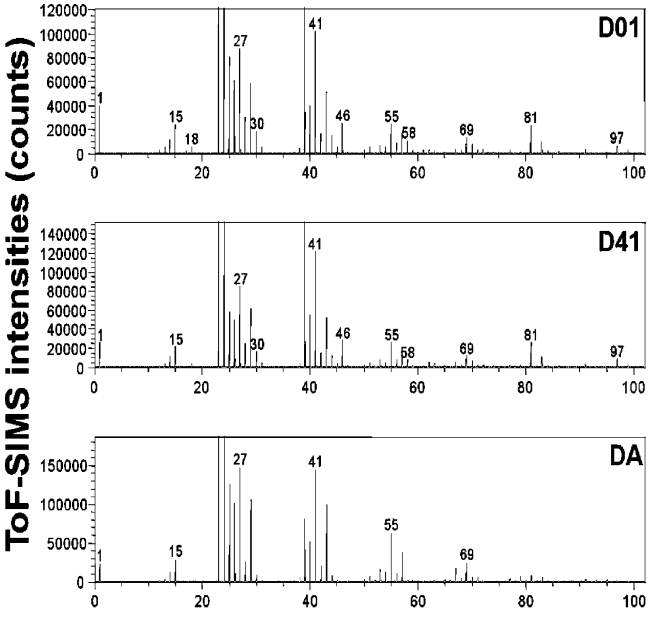

	$^{23}Na^+$ intensity	$^{24}Mg^+$ intensity	$^{39}K^+$ intensity
D01	2200000	700000	330000
D41	1900000	350000	330000
DA	1400000	450000	90000

Figure 4. Positive ToF−SIMS spectra for the D01, D41, and DA bacterial strains.

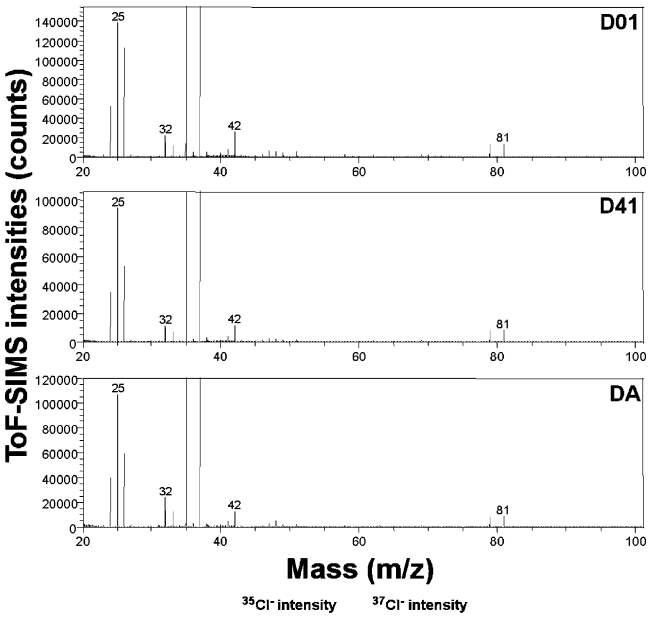

	$^{35}Cl^-$ intensity	$^{37}Cl^-$ intensity
D01	1225000	565000
D41	640000	233000
DA	630000	230000

Figure 5. Negative ToF−SIMS spectra for the D01, D41, and DA bacterial strains.

the Cl^- isotopes coming from the sea salts, the Y scales were again saturated. The Cl^- isotope absolute intensities are reported below the figure. As in the case of the positive spectra, there is no major difference between the three bacterial strains. The negative spectra are dominated by the O^- and OH^- peaks (not shown) and by the Cl^- isotopes (at masses 35 and 37 *m*/*z*). Many other inorganic peaks are also detected such as Br^- isotopes (at the masses 79 and 81 *m*/*z*), P^- (31 *m*/*z*) and its combination with O (PO^-, PO_2^-, and PO_3^- at the masses 47, 63, and 79 *m*/*z*), S^- (32 *m*/*z*) and its combination with O (SO^-, SO_2^-, SO_3^-, HSO_3^-, SO_4^-, and HSO_4^- at the masses 48, 64, 80, 81, 96, and 97 *m*/*z*), and the combinations between N and O (NO^-, NO_2^-, and NO_3^- at the masses 30, 46, and 62 *m*/*z*). Several combinations containing the Cl isotopes are detected: ClO^- (at the masses 51 and 53 *m*/*z*), $NaCl^-$ (at the masses 57.959 and 60 *m*/*z*), Cl_2^- (at masses 70, 72, and 74 *m*/*z*), and $NaCl_2^-$ (at masses 93, 95, and 97 *m*/*z*).

Many organic hydrocarbon peaks ($C_xH_y^-$) are detected. There are for instance the peaks at the masses 24, 25, 36, 38, 49, 51, ... *m*/*z* that correspond to C_2^-, C_2H^-, C_3^-, $C_3H_2^-$, C_4H^-, and $C_4H_3^-$, respectively. Nitrogen peaks are observed at the masses 15, 26, 27, and 42 *m*/*z* that correspond to NH^-, CN^-, CNH^-, and CNO^-, respectively. These peaks are always detected on proteins and amino acids; they are not strictly chemically specific because some other compounds, though not likely present in our case, would give the same, e.g., phthalocyanine or nitroperylene. Some oxygenated peaks are detected at the masses 31, 31.99, 40, 41, 45, 58.005, 59, and 71 *m*/*z* and correspond to CHO^-, O_2^-, CO^-, COH^-, $COOH^-$, $C_2H_2O_2^-$, $C_2H_3O_2^-$, and $C_3H_3O_2^-$, respectively.

Because no difference could be directly deduced from the spectra, comparison between relative intensities (semiquantitative approach) was needed. The normalization procedure for each group of peaks, explained in the Experimental Section, is governed by the changes in intensity of the most intense peaks as compared to the ones of the salts. The relative intensities of the following ions are displayed in Table 2.

(i) For positive secondary ions, one considers the sum of the nitrogenized peaks (NH_3^+, NH_4^+, CH_4N^+, CH_5N^+, $C_2H_6N^+$, $C_2H_8N^+$, $C_3H_8N^+$, $C_4H_{10}N^+$, $C_5H_{10}N^+$, $C_5H_{12}N^+$, $C_6H_{10}N_2^+$, $C_8H_{10}N^+$, $C_9H_8N^+$, $C_8H_{20}N^+$, and $C_8H_{10}NO^+$), the sum of the oxygenated peaks (CH_3O^+, $C_2H_5O^+$, $C_3H_7O^+$, and $C_4H_9O^+$), the sum of the aliphatic hydrocarbon peaks ($C_2H_3^+$, $C_2H_5^+$, $C_3H_3^+$, $C_3H_5^+$, $C_3H_7^+$, $C_4H_5^+$, $C_4H_7^+$, $C_5H_9^+$, and $C_7H_{11}^+$), and $Na_3SO_4^+$.

(ii) For negative secondary ions, one considers the sum of NH^- and CNO^-, $COOH^-$ or $R-COOH^-$ (R = H, CH_2, or C_2H_2), SO_x^- (SO_2^-, SO_3^-, SO_4^-, and HSO_4^-) and C_2OH^-.

As seen in Table 2, which summarizes the relative intensities of the most relevant ToF−SIMS signals, the sum of the positive nitrogenized peaks and that of NH^- and CNO^- are significantly lower for the DA bacterial strain than those of the two other bacterial strains. Conversely, D41 is the one bearing the highest fraction of nitrogenized functions.

For the oxygenated functions, it is necessary to differentiate the functions containing two oxygens ($R-COOH^-$) from those containing only one (C_2OH^- and $C_xH_yO^+$). The carboxylic functions are the most intense on the D01 bacterial strain compared to the D41 and DA bacterial strains (which are close together). In the case of the functions with one oxygen (alcohol, ketone, ether, ...), the C_2OH^- peak is very similar on the three strains. Conversely, the DA bacterial strain exhibits the weakest relative intensities of the $C_xH_yO^+$ peaks; they are the most intense on D41 and intermediate on D01.

The relative intensities of the aliphatic hydrocarbon peaks follow the following order, with rather slight differences between each other: DA > D41 > D01.

For the sulfates (SO_x^- and $Na_3SO_4^+$ peaks), large differences appear, their intensities are much higher for DA than for the two other strains. The large error bar reflects important inhomogeneity of these compounds at the surface. The sulfate signals for D01 and D41 bacterial strains are similar and much weaker than for DA.

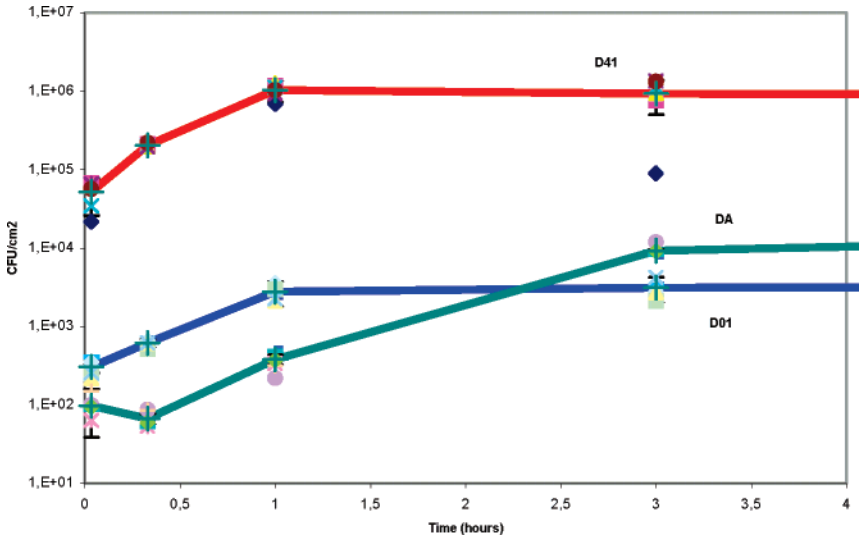

Figure 6. Adhesion curves of the three marine bacterial strains on stainless steel as a function of time. Viable strains were counted following the procedure described in the experimental part.

TABLE 2: Relative Intensities of Some Characteristic Secondary Ions and Chemical Functions (See Text for the Calculation Procedures)

	$NH^- + CNO^-$	sum positive nitrogenized peaks	C_2OH^-	$R-COOH^-$	sum positive oxygenated peaks	sum positive aliphatic peaks	SO_x^-	$Na_3SO_4^+$	PO_2^-
D01	1.30 ± 0.22	4.38 ± 0.36	0.229 ± 0.045	0.228 ± 0.017	0.860 ± 0.019	29.7 ± 1.6	0.0756 ± 0.0227	0.0336 ± 0.0123	0.0469 ± 0.0158
DA	1.07 ± 0.17	2.82 ± 0.42	0.190 ± 0.016	0.140 ± 0.013	0.673 ± 0.091	36.8 ± 2.0	0.185 ± 0.138	0.184 ± 0.105	0.0212 ± 0.0056
D41	1.40 ± 0.10	5.12 ± 0.48	0.168 ± 0.023	0.122 ± 0.006	0.946 ± 0.071	33.8 ± 1.9	0.0495 ± 0.0152	0.0551 ± 0.0075	0.0176 ± 0.0046

TABLE 3: Total Number of Cells (Viable + Nonviable) Measured on Stainless Steel after 3 h Immersion

D01	DA	D41
$1 \times 10^5 \pm 3 \times 10^4$	$2 \times 10^5 \pm 7 \times 10^4$	$2 \times 10^7 \pm 4 \times 10^6$

The relative intensity of PO_2^- is, for the D01 bacterial strain, twice as high as for D41 and DA.

2. Analysis of the Stainless Steel Surfaces after Bacterial Adhesion. a. Kinetics of Adhesion. Figure 6 shows the number of viable cultivable cells (in CFU) on a 1-cm^2 stainless steel surface after increasing the immersion time in a sterile artificial seawater bacterial solution and rinsing, estimated after spreading on a culture medium. Although D01 adheres more quickly than DA on the surface, the amounts of these two strains are very similar after 3 h contact time. The strongest differences appear with D41; from a few minutes to 4 h, the amount of D41 cells is more than 2 orders of magnitude higher than the other two cell lines. Note that for D41 and D01, the plateau is reached after 1 h of immersion, whereas the amount of viable DA cells still increases up to 3 h of contact time.

Some punctual adhesion tests were performed on other substrates, Teflon and glass, which are hydrophobic and hydrophilic, respectively. The same 10^2 factor was observed between the total amount of D41 bacteria and DA or D01 on all types of surface.

As seen in Table 3, whatever the strain, the total number of cells on the surface is higher than the number of viable ones by a factor close to 10^2 and always 10^2 higher for the D41 strain.

b. FT-IRRAS Analysis. Figure 7 shows the IRRAS spectra of the stainless steel surface after 3 h of immersion in bacterial solutions, rinsing, and drying under clean air. In the insert, the low-intensity spectra are enlarged in the *y* direction. These spectra demonstrate that bacteria are indeed present on the surfaces, showing all fingerprint absorption bands. Here again, the intensities of the bacteria signals are ca. 2 orders of magnitude higher in the case of the D41 cell, compared to the two other ones.

c. XPS Analysis. Table 4 summarizes the intensities of the metal substrate peaks as well as the one of carbon, oxygen, and nitrogen 1s peaks. The attenuation of the signals from the substrate is 1 order of magnitude stronger, after adhesion of D41, than with the two other strains. This demonstrates the considerably stronger adhesion of this type of cells on the surface. Intensities of the C 1s, N 1s, and O 1s signals from the bacteria confirm this conclusion.

Note, however, that the metals are still detected, suggesting that the average thickness of the layer is below 10 nm. In consideration of the size of the bacteria, 1−1.5 μm for the three of them, one may conclude that the layer is heterogeneous, leaving some fractions of the surface uncovered while others are likely to be totally shielded by organic material.

d. SEM Surface Characterization. SEM images of the stainless steel surfaces after 3 h of contact in artificial seawater containing bacteria (10^8 CFU/mL) led to the following data: while a few cells were hardly detected on the stainless steel surface after 3 h in DA or D01 solutions, the coverage appears to be much higher after immersion in D41 solutions. The total number of cells was estimated to be equal to 10^5 cells/cm^2 for D01 and DA and 2×10^7 cells/cm^2 for D41.

Discussion

The aim of this study was to gain a chemical characterization of the core shells of three marine bacteria and try to make clear some correlations with their adhesion properties on stainless steel in artificial seawater. The three utilized techniques, ToF−SIMS, XPS, and FT-IR, provide characterizations of the cells at various depths, and though some apparent discrepancies may exist between the nature of the predominant chemical groups, the O/C XPS ratio and the total oxygenated ions for instance, some clear tendencies emerge from all data. Table 5 summarizes

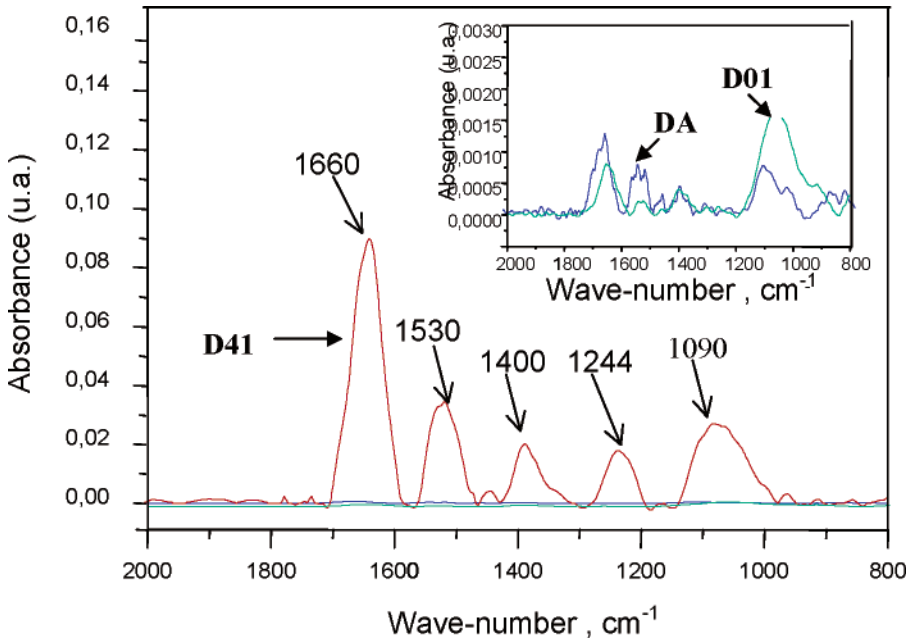

Figure 7. IRRAS spectra of the stainless steel surface after 3 h of contact in a 10^8 CFU/mL bacterial solution in artificial seawater. The samples were rinsed in NaCl solution and dried before analysis. Here the signals originate from the total number of cells (viable or not).

TABLE 4: Intensities of the Substrate, Carbon, and Nitrogen XPS Main Peaks (Raw Data) after 3 h Contact in Bacteria Solutions, Rinsing in Artificial Sea Water

	Fe + Cr	Σ C 1s	Σ N 1s	Σ O 1s
D01	101 471	20 044	2 886	71 348
DA	82 304	19 888	3 752	52 908
D41	7 770	36 466	11 852	30 885

TABLE 5: Main Tendencies Deduced from XPS and ToF−SIMS Results, +, ++, (−), −, and −− Being Used to Compare Intensities or Intensity Ratios between Each Others

		D01	D41	DA
XPS	N/C	+	+	−
	O/C	−	−−	+
	S/C	−−	−−	++
	NC═O/ΣC	+	++	−
ToF-SIMS	ΣN^+	+	+(+)	−
	ΣO^+	+	+	−
	Σ COOH	+	−	−
	$\Sigma C_{aliphatic}$	(−)	+	+(+)
	$Na_3SO_4^+$	−	−	++
	CNO^-	+	+(+)	−
	ΣO^- (excluding sulfates)	+	−	−

the main tendencies that can be deduced when comparing the XPS and ToF−SIMS results for the three micro-organisms.

The total amount of surface oxygen maximum on DA from XPS data (see in Table 1), cannot be explained by considering organic materials only, since the COOH XPS and ToF−SIMS signals are far from being the most intense on that bacteria.

An explanation is brought up by the ToF−SIMS sulfate signal, dominating on DA compared to the other strains (see in Table 2). Sulfur, from sulfates (EB = 170 eV), was also found to be maximum on DA from XPS analyses. One can conclude that the DA cell is bearing a relatively high density of sulfates on its surface. A simple calculation of the oxygen contribution intensity, expected to be associated to sulfates, could be done.[1] ($^1I_O/\alpha_O \approx 4I_S/\alpha_S$, where α_O and α_S are the oxygen and sulfur Scoffield factors, respectively.) The oxygen vs sulfur intensity ratio, very close to 4, confirms that almost all the oxygens on the DA surface come from the sulfates. Note also that the oxygen XPS intensity is likely to include a small contribution from the substrate underlying the organic layer.

Besides that, DA is the strain that yields the most intense aliphatic carbon ToF−SIMS signal. It is also the one for which the low-energy contribution to the XPS C 1s peak is the strongest, suggesting the presence of lipids or phospholipids on its outmost layer. This is in agreement with the rather high contributions of the O 1s XPS peak at 531.5 and 533.1 eV for that strain.

XPS and ToF−SIMS data are in perfect agreement to show that the D01 is the cell having the highest amount of COOH groups on its surface. This, together with the relatively low contribution of the nonprotonated nitrogen, can be correlated to the presence of polysaccharides.[28]

Another set of information is the XPS N/C ratio as well as the C 1s peak contribution at ca. 287.8 eV (attributed to NC═O groups) and the ΣN^+ and CNO^- ToF−SIMS intensities. One has to keep in mind that the differences between the three strains are small, sometimes included in the error bars. However, statistically these three data, all slightly higher for D41, may suggest the presence of proteinaceous residues on its core shell. Important is to note that no other distinct type of compounds was clearly identified on D41, whereas D01 is likely to bear both significant amounts of proteins and carbohydrates.

The combination of XPS and ToF−SIMS analyses was necessary to identify the predominating functions on each of these strains and to make clear some differences. Very schematically, the surface characterizations of the three bacterial strains enable us to conclude that D41 is surface enriched in proteins, DA in sulfates, and D01 both in proteins and carboxylic groups, i.e., polysaccharides.

In consideration of the MATS data, briefly recalled in the Introduction, it is tempting to correlate the strong electron-donor and electron-acceptor character of D01 and DA to the presence of carboxylic groups and sulfates, respectively, on their surfaces;[29] conversely, D41, apparently bearing more proteins in its topmost layer, has, as expected, weaker electron donor and electron acceptor characters. If the cell surface hydrophobicity is indeed often associated to a high N/C surface ratio, corresponding to a high concentration in proteinaceous groups,[30] this

is obviously the case of D41. The high amount of NH_2 in the surface layers of D41 may indeed suggest a higher hydrophobicity.[30] Bonnaert and Rouxhet already demonstrated the relationship between the chemical composition of bacteria and their physicochemical properties;[28] in particular, they correlated the cell hydrophilicity to high concentrations of oxygen; this is obviously the case of the D01 and DA strains.

D01 is also relatively rich in nitrogen-containing compounds, likely proteins; however, it is the only cell bearing a dominant fraction of carbohydrates on its surface, known to induce strong hydrophilicity.[29,31] In the case of DA, proteins are of course likely to be important constituents of the cell, but they are "screened" by the presence of sulfates on the outmost part of the microorganism.

These differences in the superficial concentration of the three micro-organisms lead us to expect specific behaviors when interacting with solid surfaces.

Let us recall that D41 is the cell that exhibits the strongest adhesion to various types of surfaces. On stainless steel, the total number of D41 adherent cells was observed to be 10^2 higher than the one of DA or D01. Note that, contrary to expectation, D41, the apparently less hydrophilic strain, was also the one that adhered more than the others to glass.

The shape of the adhesion curves is worth discussing; one observes that, for D01 and D41, a plateau is reached after only 1 h of contact time, whereas the number of viable DA cells still increases up to 3 h; this means that either DA cells grow on the surface or that they grow in solution and consequently adhere for a longer time. The stronger viability of the DA strain, compared to the others, in the same artificial seawater medium, leads us to assess that the second reason is playing a role even if it is not the only one.

Adhesion properties of D41 and DA, though both hydrophilic, are strongly different, leading to the conclusion that the electron donor/electron acceptor capacity, i.e., under certain conditions, hydrophilicity/hydrophobicity, is not the only parameter to account for in cell adhesion on surfaces. This agrees well with Busscher et al. who concluded that the whole set of physicochemical properties has to be considered to explain bacterial cell−solid substrate interactions.[32] Similar conclusions were drawn from a more recent work by Eginton et al.;[33] these authors claim that the extent of colonization by *P. aeruginosa* or *S. epidermidis* bacterial cells is independent of substratum hydrophobicity.

Schneider also showed a lack of correlation between contact angle-derived physicochemical parameters and cell adhesion on various surfaces including stainless steel.[34]

At high ionic strength, which is the case in artificial seawater, Derjaguin−Landau−Verwey−Overbeek-type interactions (electrostatic, Lewis acid−base, and van der Waals interactions) are expected not to be determining the adhesive behavior of microorganisms to solid substrates.[35] As for hydrogen bonds, known to be determining the interaction between oxide surfaces and bacterial surface polymers such as lipopoly-saccharide,[36] they could participate in the binding of DA or D41, both producing exopolymeric substances; they could play a determining role in the remarkable adhesion of D41, since the presence of surface sulfate groups was shown to be present around DA and probably shield this type of interaction. This is in agreement with Tsuneda et al. who showed that cell adhesion to solid surfaces could be enhanced by extracellular polymeric substances, including proteins, and was not correlated to hydrophobicity/hydrophilicity.[37] Note eventually the case of a soil bacterium, *Azospirillum brasilense*: its adhesion on polystyrene provided direct evidence of the role of extracellular proteins.[38]

Conclusion

The physicochemical surface properties of three bacterial strains of marine origin were investigated by combining three complementary surface analytical techniques. Adhesion of these bacteria was investigated in artificial seawater, and correlations between these two sets of data were attempted. The three Gram-negative marine strains appear to bear distinct functions on their core shells: the presence of carbohydrates in the external layers of the D01 micro-organism was demonstrated, whereas DA is enriched in sulfates and D41 in proteins.

For all studied bacterial cells, adhesion reached a plateau after only 1 h for D01 and 41 and 3 h for DA of contact time; the highest adhesion density was observed for D41, the cell on which only proteinaceous materials could be clearly evidenced.

The influence of cell-surface composition on the bacterial adhesion was demonstrated from XPS and ToF−SIMS data. Conversely, the role of surface/cell electron-donor/electron-acceptor or hydrogen-type interactions could not be evidenced in these experiments.

Acknowledgment. Ifremer and the Bretagne region in France are fully acknowledged for financial support of C. Rubio, Ph.D. We thank F. Mazeas for her precious contribution to the experiments.

References and Notes

(1) Otto, K.; Elwing, H.; Hermansson, M. *Colloids and Surfaces B: Biointerfaces* **1999**, *15*, 99.
(2) Coquet, L.; Cosette, P.; Beucher, G. A.; Saiter, J. M.; Jouenne, T. *Colloids Surf., B* **2002**, *26*, 373.
(3) Jucker, B. A.; Harms, H.; Hug, S. J.; Zehnder, A. J. B. *Colloids Surf., B* **1997**, *9*, 331.
(4) Mei, H. C. v. d.; Vries, J. d.; Busscher, H. J. *Surf. Sci. Rep.* **2000**, *39*, 1.
(5) Dufrêne, Y.; Wal, A. v. d.; Norde, W.; Rouxhet, P. G. *J. Bacteriol.* **1997**, *179*, 1023.
(6) Briandet, R.; Herry, J. M.; Bellon-Fontaine, M. N. *Colloids Surf., B* **2001**, *21*, 299.
(7) Grasland, B.; Mitalane, J.; Briandet, R.; Quemener, E.; Meylheuc, T.; Linossier, I.; Vallee-Rehel, K.; Haras, D. *Biofouling* **2003**, *19*, 307.
(8) Sharma, P. K.; Ras, A.; Raos, K. H.; Forssberg, F. S. E. *Hydrometallurgy* **2003**, *71*, 285.
(9) Boonaert, C. J. P.; Dufrêne, Y. F.; Derclaye, S. R.; Rouxhet, P. G. *Colloids Surf. B* **2001**, *22*, 171.
(10) Tyler, B. J. *Ann. N.Y. Acad. Sci.* **1997**, *831*, 114.
(11) Mei, H. C. V. d.; Noordmans, J.; Busscher, H. J. *Infrared Physics* **1990**, *30*, 143.
(12) Bakker, D. P.; Postmus, R. B.; Busscher, H. J.; Mei, C. H. V. D. *Appl. Environ. Microbiol.* **2004**, *70*, 3758.
(13) Rubio, C. Compréhension des mécanismes d'adhésion des biofilms en milieu marin en vue de la conception de nouveaux moyens de prévention. Paris VI, 2002.
(14) Rougeaux, H.; Talaga, P.; Carlson, R. W.; Guezennec, J. *Carbohydr. Res.* **1998**, *312*, 53.
(15) Rienzo, J. M. D.; Nakamura, K.; Masayori, I. *Annu. Rev. Microbiol.* **1978**, *47*, 481.
(16) Wicken, A. J.; Knox, K. W. *Biochim. Biophys. Acta* **1980**, *604*, 1.
(17) Bellon-Fontaine, M. N.; Rault, J.; Van-Oss, C. J. *Colloids Surf., B* **1996**, *7*, 47.
(18) Busscher, H. J.; Belt-Gritter, B. V. d.; Mei, H. C. v. d. *Colloids Surf., B* **1995**, *5*, 111.
(19) Mei, H. C. v. d.; Belt-Gritter, B. v. d.; Busscher, H. J. *Colloids Surf., B* **1995**, *5*, 117.
(20) Rouxhet, P. G.; Genet, M. J.; VCH: New York, 1991.
(21) Compere, C.; Bellon, M.-N.; Bertrand, P.; Costa, D.; Marcus, P.; Poleunis, C.; Pradier, C. M.; Rondot, B.; Walls, M. G. *Biofouling* **2001**, *17*, 129.
(22) Briggs, D.; Seah, M. *Practical Surface Analysis by Auger and X-ray Photoelectron Spectroscopy*; John Wiley & sons: New York, 1984.
(23) Rouxhet, P. G.; Mozes, N.; Dengis, P. B.; Dufrêne, Y. F.; Guerin, P. A.; Guerin, M. J. *Colloids Surf., B* **1994**, *2*, 347.

(24) Bertrand, P.; Weng, L. T. *Mikrochim. Acta* **1996**, *13*, 167.
(25) Briggs, D.; Hearn, M. J. *Vacuum* **1986**, *36*, 1005.
(26) Bellamy, L. J. *The Infrared Spectra of Complex Molecules*; Chapman and Hall: London, 1980; Vol. II.
(27) Lavalley, J. C. *Catal. Today* **1996**, *27*, 377.
(28) Boonaert, C. J. P.; Rouxhet, P. G. *Appl. Environ. Microbiol.* **2000**, *66*, 2548.
(29) Cuperus, P. L.; Mei, H. C. v. d.; Reid, G.; Bruce, A. W.; Khouri, A. H.; Rouxhet, P. G.; Busscher, H. J. *J. Colloid Interface Sci.* **1993**, *156*, 319.
(30) Mei, H. C. v. d.; Belt-Gritter, B. v. d.; Pouwels, P. H.; Martinez, B.; Busscher, H. J. *Colloids Surf., B* **2002**, *28*, 127.
(31) Pelletier, C.; Bouley, C.; Cayuela, C.; Bouttier, S.; Bourlioux, P.; Bellon-Fontaine, M. N. *Appl. Environ. Microbiol.* **1997**, 1725.
(32) Meinders, J. M.; Mei, H. C. v. d.; Busscher, H. J. *J. Colloid Interface Sci.* **1995**, *176*, 329.
(33) Eginton, P. J.; Gibson, H.; Holah, J.; Handley, P. S.; Gilbert, P. *Colloids Surf., B* **1995**, *5*, 153.
(34) Schneider, R. P. *J. Colloid Interface Sci.* **1997**, *188*, 504.
(35) Rijnaarts, H. H. M.; Norde, W.; Brower, E. J.; Lyklema, J.; Zehnder, A. J. B. *Colloids Surf., B* **1995**, *4*, 5.
(36) Jucker, B. A.; Harms, H.; Hug, S. J.; Zehnder, A. J. B. *Colloids Surf., B* **1997**, *9*, 331.
(37) Tsuneda, S.; Aikawa, H.; Hayashi, H.; Yuasa, A.; Hirata, A. *FEMS Microbiol. Lett.* **2003**, *223*, 297.
(38) Dufrêne, Y. F.; Boonaert, C. J. P.; Rouxhet, P. G. *Colloids Surf., B* **1996**, *7*, 113.